XI. PLASMA MAGNETOHYDRODYNAMICS AND ENERGY CONVERSION*

Prof. G. A. Brown	J. F. Carson	K. S. Lee
Prof. E. N. Carabateas	A. N. Chandra	R. F. Lercari
Prof. S. I. Freedman	R. S. Cooper	W. H. Levison
Prof. W. H. Heiser	J. M. Crowley	A. T. Lewis
Prof. M. A. Hoffman	R. Dethlefsen	H. C. McClees, Jr.
Prof. W. D. Jackson	M. G. A. Drouet	S. W. Miller
Prof. J. L. Kerrebrock	D. A. East	S. A. Okereke
Prof. H. P. Meissner	J. R. Ellis, Jr.	J. H. Olsen
Prof. J. R. Melcher	M. R. Epstein	E. S. Pierson
Prof. G. C. Oates	F. W. Fraim IV	D. H. Pruslin
Prof. J. P. Penhune	J. W. Gadzuk	M. H. Reid
Prof. J. M. Reynolds III	J. Gerstmann	C. W. Rook, Jr.
Prof. A H. Shapiro	N. Gothard	A. W. Rowe
Prof. J. L. Smith, Jr.	J. B. Heywood	A. Shavit
Prof. R. E. Stickney	P. G. Katona	A. Solbes
Prof. H. H. Woodson	F. D. Ketterer	J. S. Weingrad
A. A. Aponick	G. B. Kliman	G. L. Wilson
E. R. Babcock	A. G. F. Kniazzeh	J. C. Wissmiller
M. T. Badrawi	M. F. Koskinen	B. M. Zuckerman

A. WORK COMPLETED

1. TRAVELING DENSITY VARIATIONS IN PARTIALLY IONIZED GASES

This research has been completed by R. S. Cooper and the results have been presented as a thesis with the same title to the Department of Electrical Engineering, M.I.T., in partial fulfillment of the requirements for the degree of Doctor of Science, September 1963.

W. D. Jackson

2. LIQUID-METAL INDUCTION GENERATORS

The present phase of this work has been completed by M. H. Reid and the results have been presented in a thesis entitled "Experimental Investigation of a Liquid Metal Induction Generator" to the Department of Electrical Engineering, M.I.T., in partial fulfillment of the requirements for the degree of Master of Science, September 1963.

W. D. Jackson

3. STUDY OF FLUID TURBULENCE

The present phase of this work has been completed by H. C. McClees, Jr. and the results have been presented in a thesis entitled "Study of Fluid Turbulence with 10 Megacycle Ultrasound" to the Department of Electrical Engineering, M.I.T., in partial

*This work was supported in part by the National Science Foundation under Grant G-24073, and in part by the U.S. Air Force (Aeronautical Systems Division) under Contract AF33(616)-7624 with the Aeronautical Accessories Laboratory, Wright-Patterson Air Force Base, Ohio.

fulfillment of the requirements for the degree of Bachelor of Science, September 1963.

W. D. Jackson

B. PITOT TUBE FOR USE IN MAGNETOHYDRODYNAMIC FLOW

In general, the pressure and velocity fields in an MHD flow are affected by the electromagnetic forces. Velocity measurement with an ordinary pitot tube is complicated by the interaction between the electromagnetic forces and the pressure. In some cases this interaction can be avoided by utilizing the special properties of a two-dimensional flow with the plane of flow normal to the magnetic field. In such a flow the pressure distribution on the surface of an insulating object is independent of the electromagnetic forces.

Our experimental model was a symmetrical airfoil-shaped strut with pressure taps at the stagnation point and near the point of minimum pressure. It was tested in a mercury stream of known velocity to verify the two-dimensional theory and to investigate three-dimensional effects arising as the pressure taps were moved toward the end of the airfoil. The results of the experimental and theoretical work will now be presented. A more complete treatment will be found in the author's thesis.[1]

1. Theoretical Results

In a purely two-dimensional flow with the magnetic field normal to the plane of flow, the pressure distribution on an insulating object is dependent only on the free-stream velocity. There are, however, several factors working to alter these postulated conditions. Induced magnetic fields arising from current flow tend to change the direction of the total magnetic field. These induced field components are found to be small when

$$\frac{4\mu\sigma\Delta\phi}{B_o} \ll 1,$$

where $\Delta\phi$ is the voltage drop measured between the pressure taps, B_o is the strength of the applied field, and μ and σ are the fluid permeability and conductivity, respectively.

The condition that the flow be two-dimensional may be violated by the random three-dimensional velocity perturbations present in a turbulent flow. Electromagnetic forces can suppress the onset of turbulence, thereby causing the flow pattern and pressure distribution to be dependent on the strength of the magnetic field.

The three-dimensional flow about an actual probe of finite length is perhaps the most important violation of the postulated condition of two-dimensional flow. In order to obtain an estimate of the size of this effect, the flow about the tip of the airfoil was approximated by the following crude model.

Flow above the airfoil tip was taken as the potential flow about an infinite cylinder.

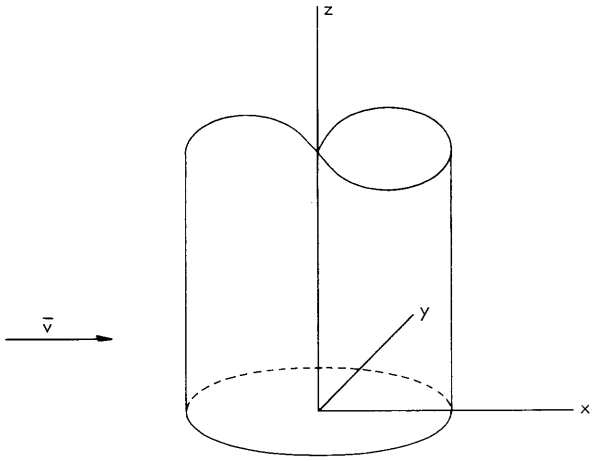

Fig. XI-1. Idealized model of airfoil tip.

Below the tip the flow was assumed to be uniform and parallel (see Fig. XI-1). Hence, the z variation in velocity is approximated as a step across the plane z = 0. Using this model for the velocity field, we estimated the current density at various heights, ℓ, above z = 0. From this current density the $\int \bar{J} \times \bar{B} \cdot d\bar{s}$ was computed along the stagnation streamlines at various heights, ℓ. This number is the change in Bernoulli number along a streamline caused by the three-dimensional flow and is given by

$$\int_S \bar{J} \times \bar{B} \cdot d\bar{s} = \sigma B_o V_\infty t \frac{\ln\left(1+\frac{2\ell}{t}\right)}{16\frac{\ell}{t}}, \tag{1}$$

where t is the thickness of the airfoil.

At the stagnation pressure tap the increase in Bernoulli number causes an equal increase in pressure because the velocity is zero. At the static pressure tap the pressure change also depends on the fluid-velocity change. Hence an accurate solution for the pressure at the static tap requires a solution for the velocity at the tip of the strut. This nearly impossible problem was ignored, and two special cases, chosen only for their simplicity, were considered.

Case 1

The increase in Bernoulli number changes only the velocity at the static tap and the pressure remains the same as for the no-field case. For this condition

$$\frac{\Delta P}{\rho V_\infty^2} = \text{CONST.} + \frac{\sigma B_o t}{\rho V_\infty} \frac{\ln\left(1+\frac{2\ell}{t}\right)}{16\frac{\ell}{t}}, \tag{2}$$

where ℓ is the distance from the end of the airfoil to the pressure taps.

Case 2

The increase in Bernoulli number changes only the pressure at the static tap and the velocity remains the same as for the no-field case. For this condition

$$\frac{\Delta P}{\rho V_\infty^2} = \text{CONST.} + \frac{\sigma B_o t}{\rho V_\infty}\left[\frac{\ln\left(1+\frac{2\ell}{t}\right)}{16\frac{\ell}{t}} - \frac{\ln\left(1+\frac{2\ell'}{t}\right)}{16\frac{\ell'}{t}}\right], \tag{3}$$

where ℓ and ℓ' are distances from the airfoil tip to the point where the streamlines passing over the stagnation and static pressure taps first touch the airfoil, ℓ' as a function of ℓ is estimated from the computed streamline over the tip of a biconvex parabolic strut in an ordinary nonmagnetohydrodynamic flow.

Equations 2 and 3 indicate that the slope of a plot of $\frac{\Delta P}{\rho V_\infty^2}$ vs $\frac{\sigma B_o t}{\rho V_\infty}$ should be a function of pressure tap position only. This function is plotted for the two cases with the experimental results in Fig. XI-2.

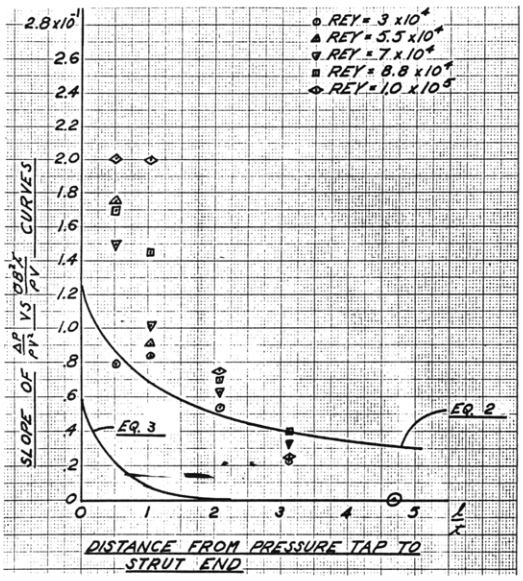

Fig. XI-2. Theoretical and experimental geometry factors.

2. Experimental Results

The dimensionless variables $\frac{\Delta P}{\rho V^2}$ and $\frac{\sigma B_o t}{\rho V}$ were calculated from the data taken. Figures XI-3 through XI-8 are plots of these variables. Each figure shows five curves for one particular geometry. Each curve is at a Reynolds number that is constant within the range specified. The maximum experimental error, ϵ, in $\frac{\Delta P}{\rho V^2}$ is given as the total height of the "I" shaped marks.

After the data for each figure were taken, the distance ℓ was reduced by cutting a small piece from the end of the airfoil. In Fig. XI-8 an attempt to restore the two-dimensional flow was made by fastening fins to the geometry of Fig. XI-6.

In general, the experimental curves are straight lines, as predicted by Eqs. 2 and 3, and the slopes increase as three-dimensional effects appear with decreasing ℓ/t. However, the curves for Reynolds number, REY = 5×10^4, in Figs. XI-3, XI-4, and XI-5 are unusual. The following explanation is proposed.

A thickening of the boundary[2] layer on the airfoil resulting from either separation or transition from laminar to turbulent flow is expected near the static pressure tap at Reynolds number 5×10^4. Since a magnetic field tends to suppress turbulence, the exact position of the thickness change is a function of both Reynolds number and magnetic field strength. Low Reynolds numbers and high magnetic fields move the transition point downstream and vice versa. It is suggested that the pressure change in the second curve of Fig. XI-3 is caused by the drop in boundary-layer thickness as the increasing magnetic field moves the transition point downstream past the static pressure tap. Such a drop in boundary-layer thickness lowers the apparent thickness of the airfoil and thus causes a rise in pressure and therefore a fall in ΔP. The consistent high and low values of $\frac{\Delta P}{\rho V^2}$ for the curves with REY greater and less than 5×10^4, respectively, are in agreement with this proposed mechanism.

As ℓ/t is reduced, the boundary-layer flow over the pressure measurement point becomes three-dimensional in character. The transition effects in the second curve of Fig. XI-3 are seen to die out in Figs. XI-4 through XI-7.

The values for the slopes of the curves in Figs. XI-3 through XI-7 are shown in Fig. XI-2 along with the theoretical values given by Eqs. 2 and 3. The agreement is poor, but that was to be expected in view of the extreme approximations used to solve the three-dimensional problem. A Reynolds number effect is suggested, but the uncertainty in measurement of the slopes tends to obscure it. Reynolds number could affect the slope through an interaction between the three-dimensional boundary-layer flow and the magnetic field, or through the effective

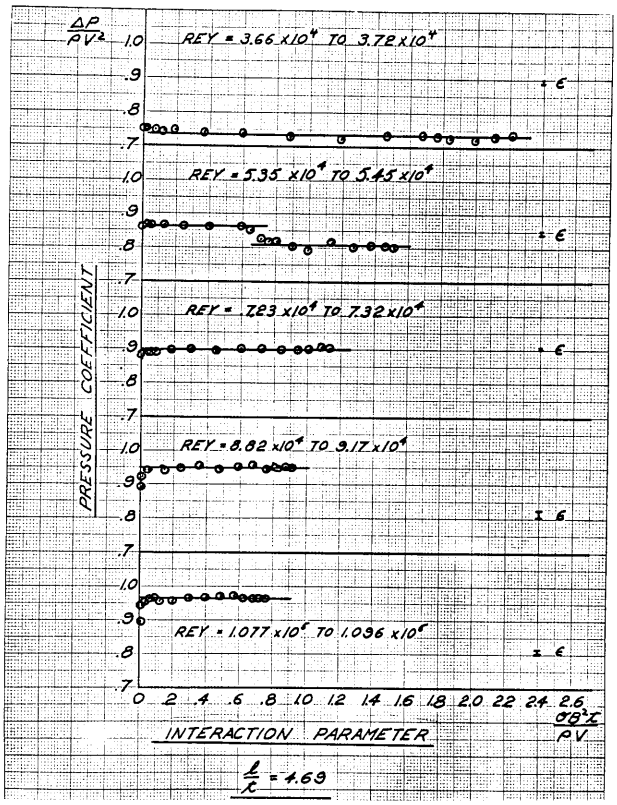

Fig. XI-3. Interaction parameter versus pressure coefficient for $\frac{l}{t} = 4.69$.

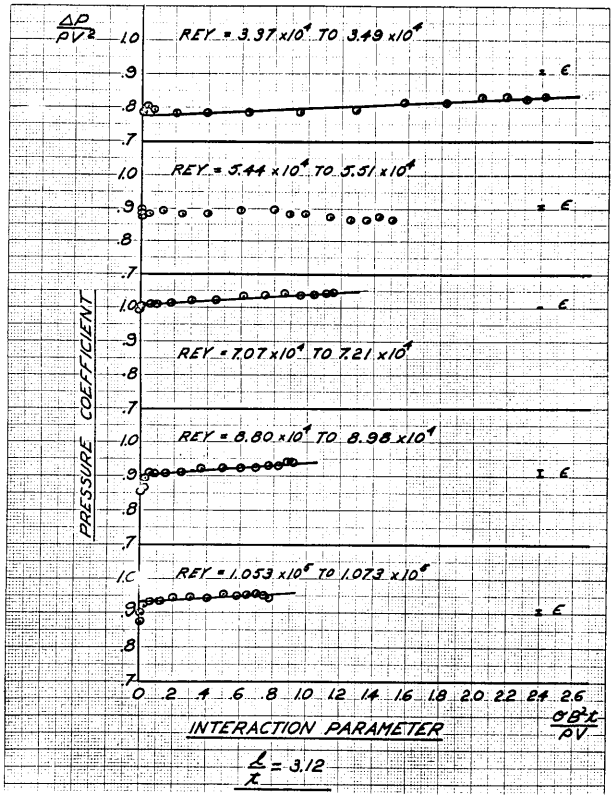

Fig. XI-4. Interaction parameter versus pressure coefficient for $\frac{l}{t} = 3.12$.

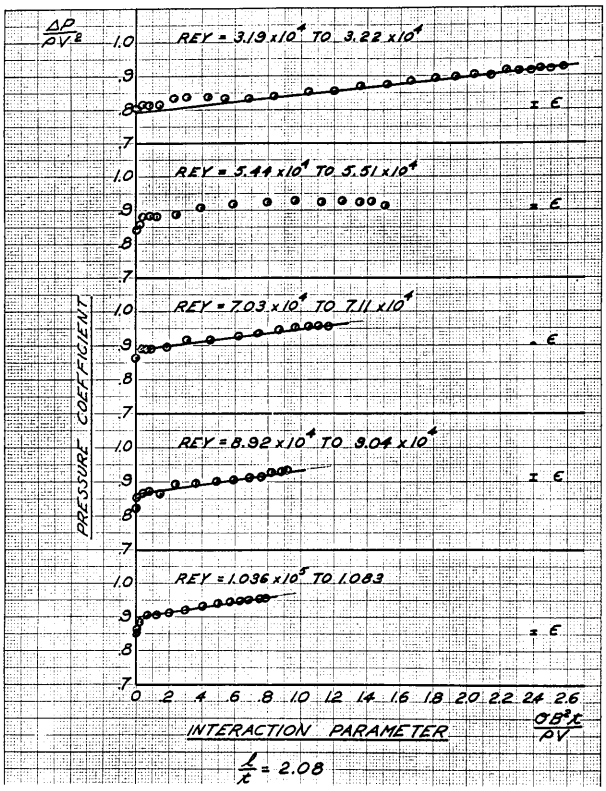

Fig. XI-5. Interaction parameter versus pressure coefficient for $\frac{\ell}{t} = 2.08$.

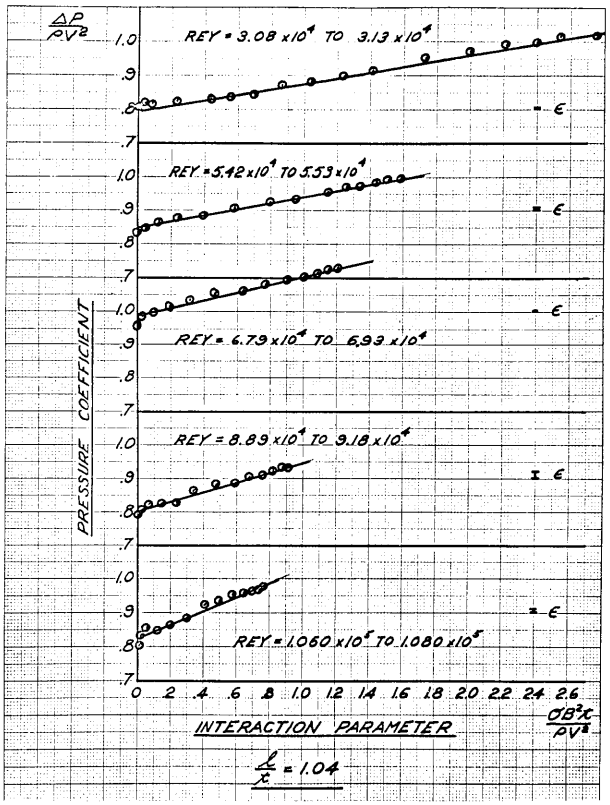

Fig. XI-6. Interaction parameter versus pressure coefficient for $\frac{\ell}{t} = 1.04$.

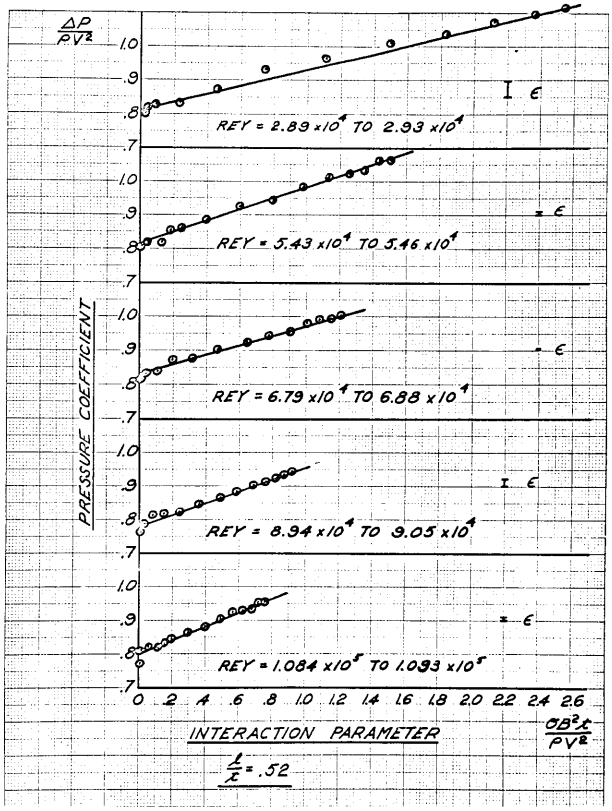

Fig. XI-7. Interaction parameter versus pressure coefficient for $\frac{\ell}{t} = 0.52$.

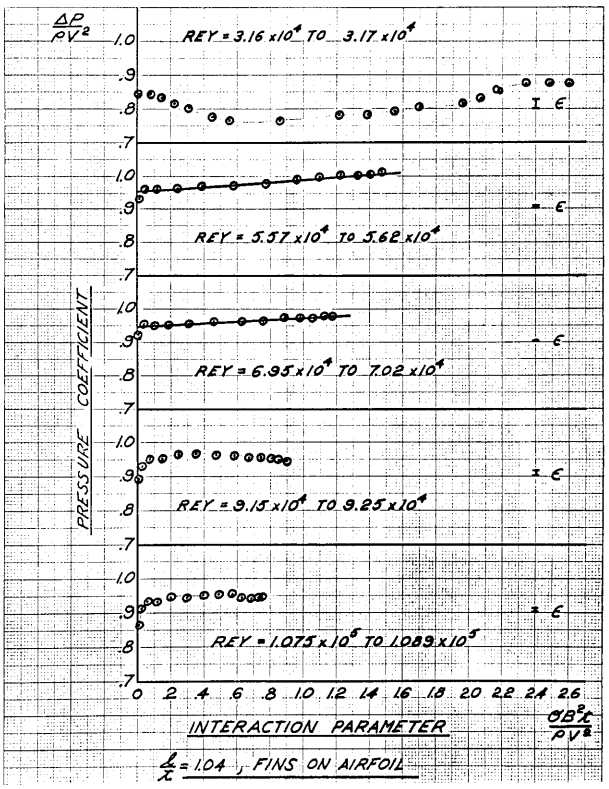

Fig. XI-8. Interaction parameter versus pressure coefficient for $\frac{\ell}{t} = 1.04$, fins on airfoil.

geometry changes caused by boundary-layer thickness changes. Note that the low Reynolds number data are closest to the curves of Eqs. 2 and 3.

3. Conclusions

The two-dimensional pitot tube has proved to be a practical device for providing a measurement of velocity independently of magnetic field strength. Its use in a three-dimensional flow is limited to cases in which the velocity is normal to the applied field, and velocity and current density changes over the length of the probe are small. It may prove to be a practical tool for measuring velocity profiles in an MHD channel flow. The main problem restricting its use is the difficulty in producing a sufficiently small probe.

J. H. Olsen

References

1. John H. Olsen, A Pitot Tube for Use in an MHD Flow, S.M. Thesis, Department of Mechanical Engineering, M.I.T., June 1963.

2. H. Schlichting, Boundary Layer Theory (McGraw-Hill Book Company, New York, 1963), Chapter 17.

3. S. Newmark and J. Collingbourne, Velocity Distribution on Untapered, Sheared and Swept-Back Wings of Small Thickness and Finite Aspect Ratio at Zero Incidence, Rep. Memor. Aero. Res. Comm. London No. 2717 (1949).

C. LARGE-SIGNAL BEHAVIOR OF A PARAMETRIC MAGNETO-GASDYNAMIC GENERATOR

Small-signal analyses and experiments previously described[1,2] have shown that a simple model can be used to predict the behavior of a parametric generator in which a plasma is used as the working fluid, and can also predict the requirements for efficient electrical operation. The geometry of the generator is shown in Fig. XI-9. The cylindrical channel of radius a has a concentric coil to produce a periodic, axial magnetic field of effective length ℓ. Periodically, batches of highly conducting plasma pass through the field region. These have a conductivity σ, a velocity v, and a Mach number M. The capacitor C is chosen so that the circuit resonant frequency is one-half the frequency of arrival of the plasma batches at the coil. The plasma enters the

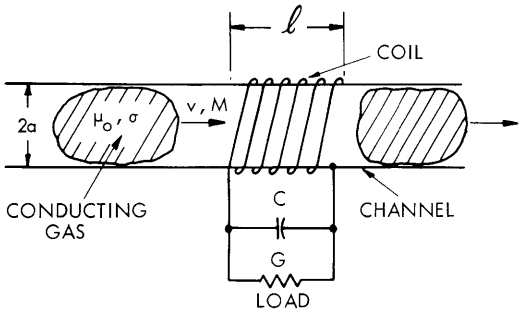

Fig. XI-9. Schematic diagram of the generator.

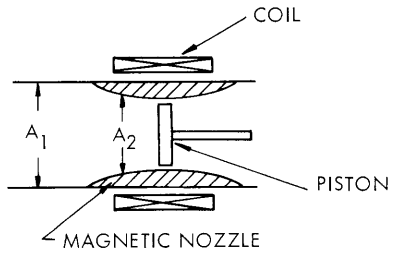

Fig. XI-10. Model for analyzing the interaction between magnetic field and plasma.

field region near the time of maximum field, and leaves at zero field when all of the electrical energy is stored in the capacitor. Thus each batch of gas does work on the field in displacing it from the channel.

The objective of this research is to extend the analysis to the large-signal case for which the magnetic field strongly affects the gas flow in order to determine

(i) Whether the requirements for the magnetic Reynolds number, $R_m = \mu_o \sigma v a$, are relaxed because of any enhancing mechanism during the interaction;

(ii) What fraction of the gas power could be extracted as useful electrical power, that is, the over-all efficiency;

(iii) The way in which the interaction between the field and the gas leads to gas behavior that limits the growth of the parametric oscillations so that a stable operating point is reached;

(iv) An estimate of the minimum size and power of a generator with the combustion gases; and

(v) The factors that control the scaling of the parametric generator.

The interaction between the magnetic field and the plasma was analyzed by using a model in which the effect of the field on the plasma is treated as a nozzle with a leaky piston as shown in Fig. XI-10. The highly conducting gas enters the field region and the flow area changes from an initial area A_1 to some new area A_2. For the analysis, R_m is assumed to be infinite so there is no magnetic-field penetration of the gas and no electrical losses in the gas. During the flow of the plasma into the field region, the magnetic flux is assumed to be constant. The area A_2 is such that the magnetic pressure, at most, balances the static gas pressure, p.

$$\frac{B^2}{2\mu_o} \leq p. \tag{1}$$

The gas flow is treated as quasi one-dimensional with constant specific heats and without ionization, dissociation, viscous losses or heat transfer. The work done in displacing the field, ΔW, equals the work given up by the gas, and determines how the gas flow behaves at any initial Mach number M_1 and initial magnetic energy storage W_{mo}.

Two cases have been considered. For pulsed flow, the region between the highly conducting plasma batches is a vacuum. For continuous flow, there is a low-conductivity gas in that region so that the magnetic field is only affected

by the periodic high-conductivity batches.

The effect of losses when $R_m \neq \infty$ are accounted for by an extension of the procedure used for the small-signal analysis.

The results of the analysis will be summarized graphically to describe the generator characteristics and provide the basis for answering the questions that prompted this investigation.

1. Generator Characteristics

a. Efficiency. The first important generator property that is not given by the small-signal analysis is the fraction of the available work which is extracted from the flow. The results of the analysis for pulsed and continuous supersonic flows are shown in Fig. XI-11. The curves shown here refer to operation at the conditions for maximum output power at each Mach number. The effects of different initial coupling, k_o^2, the ratio of channel area to effective field coil area are shown. The pulsed values are

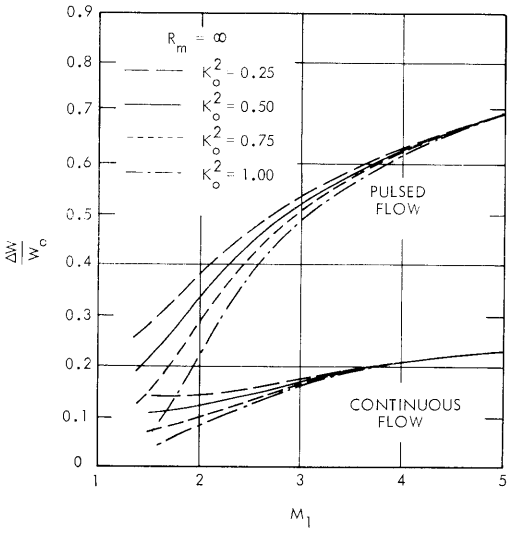

Fig. XI-11. Fraction of available work extracted for pulsed and continuous flows as a function of inlet Mach number and initial coupling.

optimistic by from 10 per cent to 20 per cent because a rarefaction wave that was included in the continuous-flow analysis was ignored for pulsed flow. With pulsed flow, there is also a rarefaction wave resulting from the free expansion of the slug and this also tends to reduce the efficiency. The effect will be greater at an inlet Mach number M_1 close to one than for higher M_1.

Subsonic flow is not attractive for several reasons. For a given stagnation

temperature, the optimum value of σv occurs in the low supersonic range so that a sacrifice in R_m is made. The results for subsonic flow indicate that only a small fraction of the energy might be extracted unless very weak coupling is used. As with turbines, most of the work comes from the kinetic energy of the flow. But the kinetic energy of a subsonic flow is only a small part of the total energy so that the efficiency for the subsonic processes is severly limited.

b. Reactive Power. We see from Fig. XI-11 that over-all efficiencies of 20 per cent for continuous flow and 40-60 per cent for pulsed flows are possible for high enough R_m. But the higher efficiencies are not obtained without a price. The reactive power that is necessary increases very rapidly with M_1 because at maximum power considerable channeling occurs, so that the coupling between the field and the gas becomes weaker. Figure XI-12 shows the ratio of reactive-to-generated power, Q, as a function of M_1 when the generator has maximum power output. The required reactive power increases with decreasing k_o^2 as shown by the curves.

For other than maximum power conditions, Q varies with the efficiency. Figure XI-13 shows the variation of Q with the fraction of energy extracted for both continuous and pulsed flows for the particular value $k_o^2 = 0.5$. The variation with k_o^2 can be seen by comparison with that in Fig. XI-12. The sharp breaks in the curves at maximum output occur because it was assumed that no reflected shock occurred in the magnetic nozzle. The envelope of the curves gives the minimum possible Q that can be obtained at any given fraction of power extracted.

c. Losses. The characteristics of the generator described previously do not include the electrical losses in the gas. It is convenient to have the properties in that form because it gives the ultimate performance and the effects of the losses can be introduced separately. The simplest form in which to present these results is a graph of the electrical efficiency η_o under various conditions and for different R_m. The over-all efficiency, the ratio of load power to power carried by the gas flow, is then $\eta_T = \eta_o \Delta W/W_o$, while the reactive power ratio in the presence of losses can be expressed as $Q_L = Q/\eta_o$. That is, the reactive power to load power ratio increases when losses are present to return part of the power to the gas flow.

Q_L must be kept small because inevitably there are losses in the coil and capacitors that limit the maximum obtainable Q to less than 500, and it is desired that more power be delivered to the load than is lost in the reactive components of the generator. Figure XI-14 shows η_o as a function of R_m for various values of k_o^2 at $M_1 = 2$ and for maximum power. Figure XI-15 shows how η_o varies with M_1 at a given R_m. The curves all approach the same limit as M_1 becomes large because the channeling reduces the coupling to such a small value that $k^2 \to 0$ effectively.

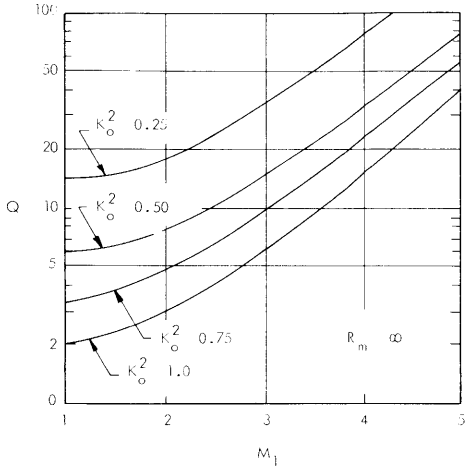

Fig. XI-12. Ratio of reactive to generated power as a function of inlet Mach number and initial coupling.

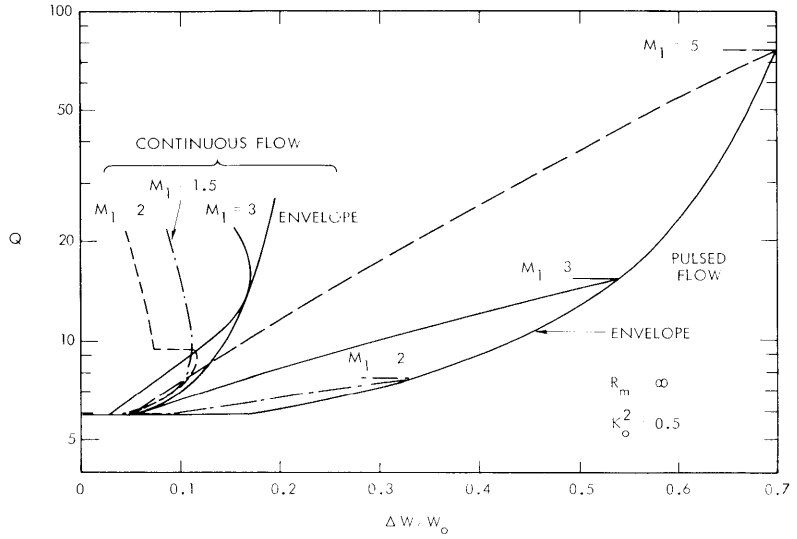

Fig. XI-13. Variation of reactive power ratio with the fraction of available power extracted.

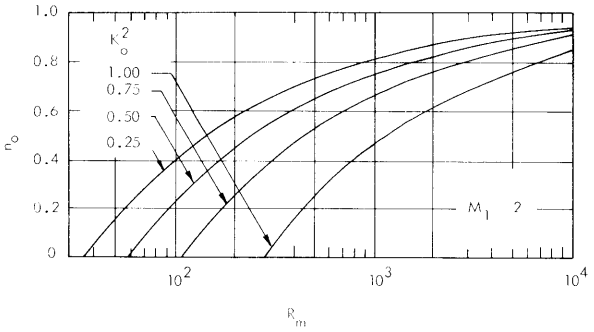

Fig. XI-14. Electrical efficiency as a function of the magnetic Reynolds number for various values of initial coupling at $M_1 = 2$.

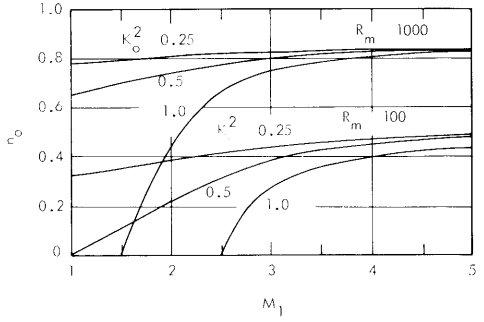

Fig. XI-15. Electrical efficiency as a function of inlet Mach number for several values of k_o^2 and R_m.

d. Rate of Build-up. Another important characteristic of the generator is the rate of growth of the oscillations. The rate of growth depends upon the loading so that with heavy loading growth may be very slow. The maximum rate of growth occurs, however, with no external load so that the only losses are in the gas. A useful measure of the growth rate is the number of cycles required for the capacitor voltage to grow to e = 2.72 times its initial value. The electrical energy in the system grows 7.4 times in the same interval. The number of pulses of conducting gas required is twice the number of cycles. As R_m tends to infinity, we get the maximum possible growth rate, and

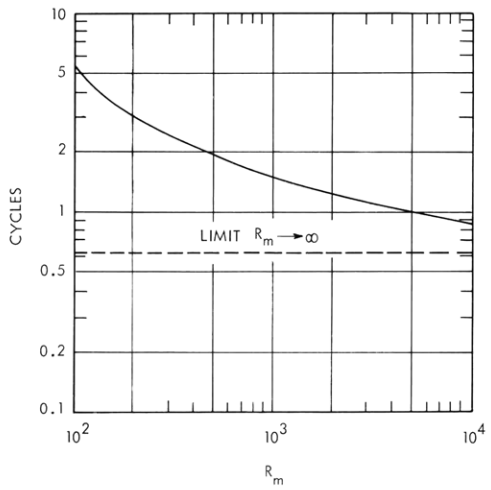

Fig. XI-16. Number of cycles required for the capacitor voltage to grow by e of its initial value as a function of the magnetic Reynolds number.

for $R_m \neq \infty$ the growth is slower. Figure XI-16 shows the number of cycles required for a voltage growth by e as a function of R_m, with the optimum geometry chosen at each value of R_m in the small-signal range. The growth rate becomes slower when channeling occurs and steady-state operation is approached. The sharpness with which the growth cuts off as the steady state is approached depends on R_m being sharper for high R_m than for low, because of the fact that the decrease in losses with channeling relative to the power generated is greater at low R_m which retards the cutoff.

e. Frequency of Operation. The frequency at which the generator will operate is determined by the frequency with which the conducting gas slugs arrive. In the small-signal limit this is given by $\omega = \pi v/2\ell$. The velocity is determined by the Mach number and temperature of the gas. If we take $M_1 = 2$, v = 2000 m/sec and $\ell/a = 2$, for $\ell = 1$ meter, $\omega = 3 \times 10^3$ sec^{-1} or f = 500 cps, and for $\ell = 10$ meters, $\omega = 300$ sec^{-1} or f = 50 cps.

These lengths correspond to channel radii a of 0.5 meter and 5 meters. For $\ell/a > 2$, the frequency is lowered, but more time is allowed for the field to diffuse in so that the losses will be higher.

When the strength of the interaction increases, the frequencies will be lower for a given initial gas velocity because the velocity through the field region will decrease. With strong channeling, the frequency could be lowered as much as 30 per cent from the value given above with the use of the initial velocity.

f. Generated Power. An idea of the power output of the generator can be obtained by considering the power available in the gas flow.

$$P = (\rho u A)\, c_p T_o = \frac{\gamma}{\gamma - 1} \frac{u A p_o}{\left[1 + \frac{\gamma - 1}{2} M_1^2\right]^{1/(\gamma-1)}} \tag{2}$$

where γ is the specific heat ratio, ρ the gas density, u the velocity, A the channel area, c_p the specific heat at constant pressure, T_o the stagnation temperature, and p_o the stagnation pressure. Table XI-1 gives the total power in the flow and the power density for various radii of the channel as determined by R_m for several values of the stagnation pressure, p_o, with the stagnation temperature of the flow taken to be ~4000°K.

Table XI-1. Flow power and power density.

Radius a (meters)	Power (watts)			Power density (watts/meter^3)		
	p_o (atm)			p_o (atm)		
	10	1	10^{-3}	10	1	10^{-3}
1	5×10^9	5×10^8	5×10^5	8×10^8	8×10^7	8×10^4
10	5×10^{11}	5×10^{10}	5×10^7	8×10^7	8×10^6	8×10^3
100	5×10^{13}	5×10^{12}	5×10^9	8×10^6	8×10^5	8×10^2

The values in Table XI-1 show that if a high enough conductivity is available, the power densities possible are much larger than for DC magnetohydrodynamic generators. Some typical values planned for DC machines are 5 megawatts/m^3 at an inlet pressure of 5.5 atm and 11 megawatts/m^3 at 8.5 atm.[3] For comparison, the values of power and power density in the table must be multiplied by the efficiency.

D-C machines must have $R_m \ll 1$ so that the ratio of magnetic to gas pressure

$B^2/2\mu_o p \gg 1$ is required for efficient operation. The parametric generator has $R_m \gg 1$ and $B^2/2\mu_o p \approx 1$ so that a smaller magnetic field is necessary to achieve a given generated power density than in the DC generator.

2. Conclusions

With the characteristics of the generator and other results of the analysis we reach the following conclusions.

(i) The conductivity and velocity requirements are not increased significantly for large-signal operation. The processes that could give enhancement are the isentropic compression of the plasma on entering the magnetic field and the effects of axial compression and rarefaction waves. The change in R_m, the important parameter, is small, however, unless the change in conductivity with temperature is stronger than the 3/2 power. This is only true at low temperatures and low fractional ionization. In order to keep the generator size down, it is necessary to operate at as high a temperature as possible so that the conductivity is governed by the fully ionized case, $\sigma \sim T^{3/2}$, and no enhancement is expected from the isentropic compression. The effect of axial waves is too small to make a significant change in R_m.

(ii) Forty per cent of the gas power might be extracted for pulsed flows, and approximately 20 per cent for continuous flows. These are values that might be expected if R_m is very high. The limiting values are shown in Fig. XI-11. The estimate for pulsed flow has been reduced from the value on the graph to account for some of the effects of the rarefaction waves that were neglected in the analysis.

(iii) To achieve good over-all efficiency, the reactive power to load power ratio would have to be approximately 10, which is considerably greater than the minimum possible value of 2. For $R_m = \infty$, Fig. XI-12 shows that Q increases with M_1, while Fig. XI-11 shows that to get an efficiency of 40-60 per cent, M_1 must be in the range 3-4, which means a Q near 10. Of course, Q can be made smaller by using a lower Mach number flow, but then the efficiency is decreased. With losses the situation is worse. For $R_m = 1000$, Fig. XI-15 gives $\eta_o \approx 0.8$, which means that the over-all efficiency decreases and Q_L increases 25 per cent. Since $R_m = 1000$ is optimistic at this time and $k_o^2 = 1$ could not be reached, it is safe to conclude that to get an over-all efficiency of 40 per cent a Q_L of at least 10 is required. For continuous flow a Q_L of 10 is required to get 20 per cent efficiency.

(iv) The minimum size generator that could be constructed for use with combustion gases is approximately 16 meters in diameter and several times as long. Because there is negligible enhancement of R_m as a result of the interaction, a minimum R_m of approximately 100 is still required for the generator. To obtain the size, additional information is required. Table XI-2 gives several fuel-oxidant systems that could possibly be

used along with the σv-product obtainable. If the fuel is burned completely before expansion, there will be an optimum M_1 to maximize σv. For $\gamma = 1.4$ and $\sigma \sim T^{3/2}$, this occurs for $M_1 = 1.3$. The σv-products in Table XI-2 could possibly be increased by a factor of 2 by burning additional fuel during the expansion and expanding to a higher velocity. The last column gives the radius for $R_m = 100$. These figures show that for equilibrium ionization, the only hope is to burn a fuel such as cyanogen at an extremely high temperature. The gas temperature would then be higher than the walls could withstand except for short-duration emergency duty.

Table XI-2. Statistics for several fuel-oxidant systems.

Fuel-Oxidant	Temperature	Seed	σ (mho/m)	σv (mho/sec)	a (m)
Acetelyne-oxygen[4]	3600°K	C_s	270	2.3×10^5	350
Fuel oil-oxygen[5]	3500°K	K	300	2.8×10^5	280
Tetracyanoethelene-hexanitroethane[4]	3500°K	C_s	5×10^3	4.3×10^6	18
Cyanogen-oxygen[4]	4850°K	C_s	10^4	10^7	8

The efficiency of the generator at $R_m = 100$ would be approximately 3 per cent for continuous flow, and 7 per cent for pulsed flow, with the optimum occurring about $M_1 = 1.5$. At higher Mach numbers, R_m decreases so that it is only advantageous to increase M_1 when R_m is near 1000 when the power extracted from the flow increases faster than the electrical efficiency decreases.

For the generator of 16-meter diameter, Table XI-1 indicates that the power output with the efficiencies given above would be ~2000-4000 megawatts with a stagnation pressure of 1 atmosphere.

(v) In order to compare two geometrically similar generators the dimensionless parameters that must be held constant are:

(a) magnetic Reynolds number, R_m

(b) Mach number, M_1

(c) ratio of specific heats, γ.

The previous analysis has shown that the generator losses are a function of R_m, while the gas behavior during the interaction depends strongly on M_1 for the amount of channeling and the pressure rise. The specific-heat ratio has been assumed to be $\gamma = 1.4$ throughout. This value is between that for noble gases and combustion gases. For a smaller value of γ, more of the energy is thermal at a given Mach number. This means

that σv would maximize at a higher M_1. The amount of channeling and the pressure rise are nearly the same for different values of γ at the same M_1. The total power carried by the flow, however, must be greater for smaller γ in order to extract the same amount of power. For $M_1 = 2$, the fraction of available energy extracted is approximately 10 per cent larger for $\gamma = 1.67$, and 30 per cent smaller for $\gamma = 1.2$ than the corresponding value for $\gamma = 1.4$. In order to get the same fraction of energy extracted for $\gamma = 1.2$, the generator would have to operate at a higher Mach number and with larger channeling so that the reactive power required would be increased.

A. T. Lewis

References

1. G. L. Wilson, A. T. Lewis, and H. H. Woodson, Quarterly Progress Report No. 67, Research Laboratory of Electronics, M.I.T., October 15, 1962, p. 96.

2. H. H. Woodson, G. L. Wilson, and A. T. Lewis, A Study of Magnetohydrodynamic Parametric Generators, presented at the Third Symposium on the Engineering Aspects of Magnetohydrodynamics, Rochester, New York, March 1962.

3. L. P. Harris, MHD Power Generation – An Application for Magnetohydrodynamics, Report 60-RL-2515G, General Electric Research Laboratory, Schenectady, New York, September 1960.

4. T. R. Brogan, A. R. Kantrowitz, R. J. Rosa, and Z. J. J. Stekly, Progress in MHD Power Generation, Engineering Aspects of Magnetohydrodynamics, edited by C. Mannal and N. Mather (Columbia University Press, New York, 1962).

5. M. S. Jones, Jr., V. Blackman, and C. McKinnon, Research on the Physics of Continuous and Pulsed MHD Generators, Report No. 632, MHD Research Inc., Newport Beach, California, February 1963.